P.1.5 *Presented at the 16th Conference on Satellite Meteorology and Oceanography, Phoenix, AZ, 1/12-15/2009*

Rainfall measurement with space-borne X-band synthetic aperture radars: A new opportunity

James A. Weinman[1], Frank S. Marzano[2], Saverio Mori[2], William J. Plant[3], Ziad S. Haddad[4], Stephen L. Durden[4], Alberto Mugnai[5]

1) Atmospheric Science Department; University of Washington, Seattle, WA 98195-1640;
2) Department of Electrical Engineering, Via Eudossiana 18, University of Rome, "La Sapienza", 00184 Roma, Italy.
3) Applied Physics Laboratory, University of Washington, Seattle, WA 98195,
4) Jet Propulsion Laboratory, 4800 Oak Grove Ave, Pasadena, CA 91109
5) Atmospheric Physics Institute, Via Galileo Galilei C.P. 27, 00044 Frascati, Italy

1 ABSTRACT

Five space-borne X-band synthetic aperture radars (SARs) are now operating and several more will be aloft in the coming years. These sensors provide an opportunity to measure rainfall over both land and sea with unsurpassed ~ 200 m spatial resolution. A brief description of rainfall retrieval algorithms from such radar data, and their validation is presented.

2 INTRODUCTION

Global precipitation measurements are needed by weather and climate modelers because the release of latent heating affects the performance of such models. Precipitation measurements are also required to facilitate management strategies for hydrology, transportation, and agriculture.

Since the 1980s much of our understanding of global precipitation has been provided by space-borne passive microwave radiometers. Unfortunately precipitation retrievals over land from those radiometer data have had limited success because they rely on the scattering properties of ice in the upper regions of precipitating clouds. Bennartz and Petty (2001) showed that the relationship between surface rainfall rates and the scattering properties of frozen hydrometeors is problematic. The ~12 km horizontal resolution of microwave radiometers also limits their sensitivity to many small convective rain cells.

This limitation can be overcome by space-based radars operating at X (~3 cm wavelength) or Ku band (~2 cm wavelength). The Ku band Precipitation Radar (PR) aboard the Tropical Rainfall Measurement Mission (TRMM) satellite has provided unique precipitation measurements over land, Kummerow et al. (2000). However if significant shallow precipitation or rain cells smaller than 4 km occur, then PR may miss or underestimate the intensity of such precipitation. Durden et al. (1998).

X-band Synthetic Aperture Radars (X-SARs) are able to measure precipitation over land where the scattering and absorption of microwave radiation by rain can be measured with greater certitude than from radiometers. The high spatial (~100 m) resolution of X-SARs can provide new insights into the structure of precipitating clouds, and it permits the observation of small precipitation cells that might be missed by the PR.

C-band and L-band (~5 and ~21 cm wavelengths respectively) SARs have a long heritage of Earth observation. However such radars are relatively insensitive to rainfall. Atlas and Moore (1987), Jameson et al.

Corresponding author address: James A. Weinman, Atmospheric Sciences Department, University of Washington, Seattle, WA 98195 e-mail <weinman@atmos.washington.edu>

(1997), Moore et al. (1997) Melsheimer et al. (1998) and Alpers and Melsheimer (2004) showed that the shorter wavelengths of X-SARs enabled them to respond to rainfall. The Shuttle Missions STS-59 and 68 of 1994 and the STS-99 Shuttle Radar Topography Mission (SRTM) of 2000 carried the first X-SAR along with L and C band SARs, Jordan et al. (1995).

Several X-SARs that are now and, will soon be placed in orbit provide a new opportunity to measure precipitation from space. The Constellation of Small Satellites for Mediterranean basin Observations, or COSMO-SkyMed (CSK) has been developed by the Agenzia Spaziale Italiana (ASI), Caltagirone et al. (2007). Three of four of those satellites are already aloft. The TerraSAR-X (TSX) was launched on June 15, 2007 by the Deutsches Zentrum f. Luft u. Raumfahrt (DLR), Buckreuss et al. (2003). Another X-SAR will be lunched by DLR by 2009. The TecSAR (SAR Technology Demonstration Satellite) was launched by the Israeli Ministry of Defense on January 21, 2008. Sharay and Naftaly (2006). And the Korean Aerospace Research Institute (KARI) plans to launch the KOrea Multi-PurposeSATellite–5 (KOMPSAT-5) near the end of the decade.

3 PRINCIPLES OF PRECIPITATION RETRIEVAL

SARs have been designed for Earth surface remote sensing, and not for atmospheric applications as the PR was. The X-SAR observation geometry produces oblique rather than nadir views that require more complex computations to retrieve rainfall distributions than those from conventional radars.

SARs measure the Normalized Radar Cross Section (NRCS) which is the backscattered power divided by the observed area, defined by the ground resolution, Weinman and Marzano (2008).

Fig. 1 shows a schematic view of our NRCS model. The horizontal and vertical coordinates are *x* and *z* respectively. σ^0 is the cross section of the surface. Scattering occurs within an oblique slice of thickness Δr perpendicular to the direction of propagation. The cloud top is at z_t and the freezing height is z_o, The cloud width is w. The viewing angle with respect to nadir is θ.

As the radar scans from left to right, for $\theta \le x \le (z_t - z_o)/\tan(\theta)$, the return is from the surface plus a component scattered by the frozen hydrometeors. As the scan moves between $(z_t - z_o)/\tan(\theta) \le x \le z_t/\tan(\theta)$, scattering is still from the surface and from the rain layer. Moving to the right between $z_t/\tan(\theta) \le x \le z_t/\tan(\theta) + w$, scattering by rain and the return from the surface are both attenuated so that the NRCS approaches a minimum value. Finally, for $z_t/\tan(\theta) + w \le x \le z_t/\tan(\theta) + w + z_t \tan(\theta)$, the attenuation path starts to diminish so that the scattering from the surface becomes less attenuated and the NRCS increases, returning to the background value at $z_t/\tan(\theta) + w + z_t \tan(\theta < x$..

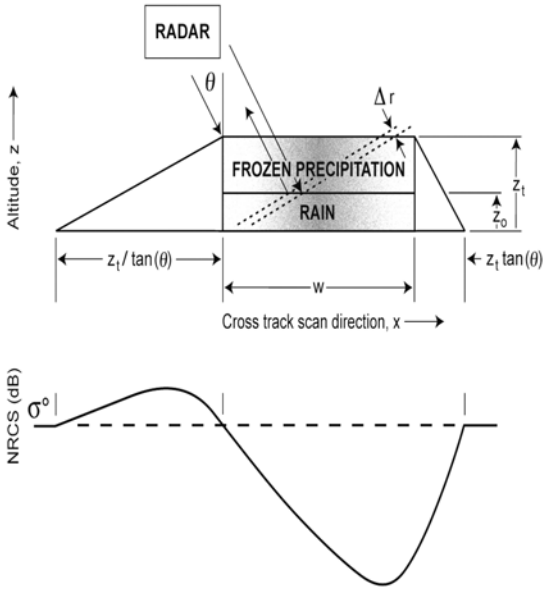

Fig. 1. (upper) Schematic view of the model used to compute the NRCS from a horizontally variable two layer precipitating cloud. **(lower)** Schematic NRCS (dB) as a function of cross-track scanning distance (km) showing enhanced values on the left of the cross-over point caused by scattering from the cloud top and attenuation from rain in the lower cloud on the right. The background NRCS is σ^0

The NRCS, σ_{SAR} is quantitatively described by the sum of two terms, *such that*:

$$\sigma_{SAR} = \sigma_{srf} + \sigma_{vol} \qquad (1)$$

where

$$\sigma_{srf} = \sigma^0 e^{-2\int_0^{\infty} k[x(z)]dz/\cos\theta}$$

is a surface contribution and

$$\sigma_{vol} = \int_0^{\infty} \eta\left[x(z)\right] e^{-2\int_z^{\infty} k[x'(z')]dz'/\cos\theta} dz$$

is a volume contribution.

Attenuation occurs in the propagation direction between the oblique slice and the radar along the entire extent of the oblique slice. The reflectivity, η (km^{-1}), depends on the radar reflectivity factor, $Z = aR^b$, where Z ($mm^6./\ m^3$) and the rain rate is, R (mm/h), The extinction coefficient is $k = cR^d$, (km^{-1}), Various types of hydrometeors, characterized by their rainfall rates contribute differently to η and k. The coefficients, *a, b, c,* and *d* are constants that depend on the particle phase, size distribution and density. Their values were assumed a priori, as is done for computations of conventional single frequency radar returns.

4 FORWARD SCATTERING MODEL

A model representing only vertically uniform rainfall was first considered by Moore et al. (1997). Our models described in Marzano et al. (2006) and Weinman and Marzano (2008) considered various vertical and horizontal distributions of liquid and frozen rainfall rate distributions represented by:

$$R(x,z) = H(x)\ V(z) \qquad (2)$$

The vertical profiles, $V(z)$, are generic and they are based on the Contoured Frequency by Altitude Diagrams (CFAD) for convective storms, Yuter and Houze (1995). The determination of the horizontal distribution, $H(x)$, is the main challenge of this study.

5 PRECIPITATION DISTRIBUTION RETRIEVALS

The solution to the radar equation consists of path integrated quantities. X-SAR rainfall retrievals are thus somewhat similar to microwave radiometric rainfall retrievals from a mathematical perspective. At least two types of solutions are feasible:

a) An analytical solution to the radar equation for vertically uniform rainfall distributions was described by Pichugin and Spiridonov (1991). That work was based on the solution of a Volterra Integral Equation (VIE) of the second kind. A recent study by Marzano and Weinman (2008) also included the effects of scattering by frozen hydrometeors.

b) Weinman and Marzano (2008) and Marzano and Weinman. (2008) found statistical relationships between moments of NRCS scans and moments of $R(x,z)$. Those moments were then used to reconstruct the $R(x,z)$. Space limitations prevent us from describing the details of the regressions between the various moments; the reader is referred to the cited articles.

5.1 Precipitation Retrieval over Land

Fig.2 (upper left) shows a 40 km wide swath of X-band imagery obtained over Amazonia, Brazil. Fig.2 (upper right) shows the NRCS values measured along the transect A-A' shown on the left. The $R(x,z)$ found by the statistical retrieval is shown in Fig. 2 (lower-left), and that found by the VIE solution is shown in Fig. 2 (lower-right).

The two methods appear to yield comparable results even though the algorithms differ mathematically. The Fig.2 (upper left) scene shows an isolated convective cell that is ~ 2 km wide along the sub-orbital direction. Such a cell would be difficult to resolve with the PR, let alone with a microwave radiometer. .

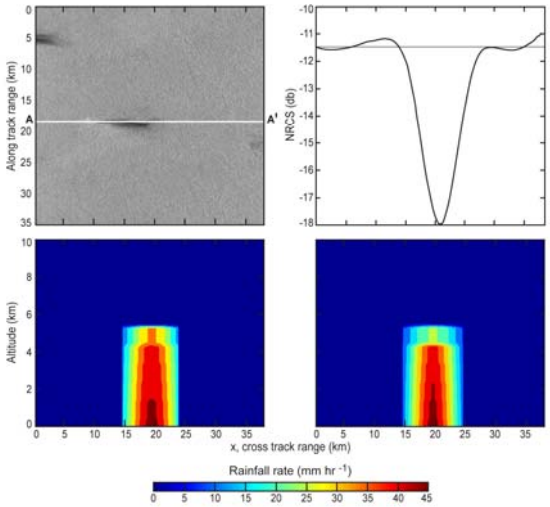

Fig. 2. ***(upper-left)*** X-SAR image of an isolated convective cell over Amazonas, Brazil (9.01°S x 68.38°W) obtained at 18:45 UTC on 15 April, 1994. The X-SAR on Shuttle Mission STS-59. viewed this scene from the left and the satellite passed from the top of the scene to the bottom. **(upper-right)** NRCS scan along the transect A-A' shown on the left. ***(lower-left)*** Comparison between the rainfall rate distribution, $R(x,z)$, retrieved by the statistical algorithm and **(lower-right)** by the VIE solution.

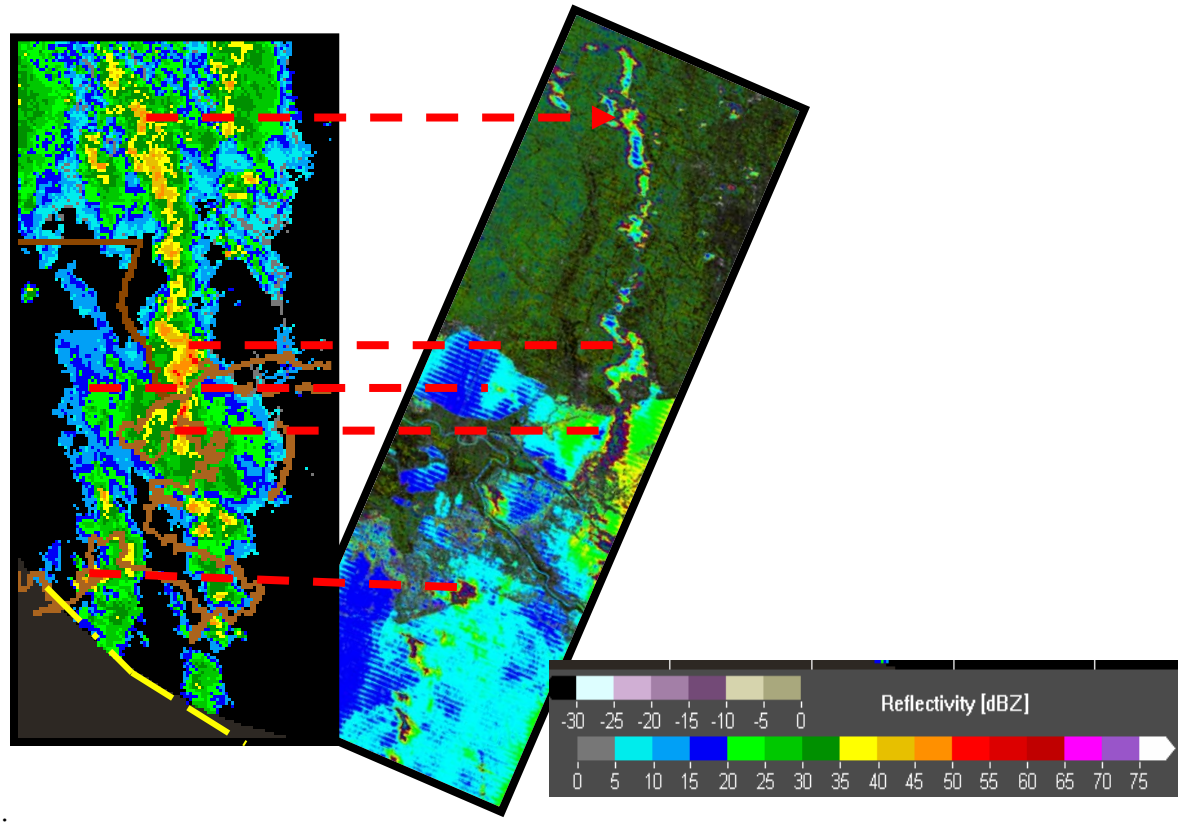

.

Fig. 3 ***(left)*** Outer rain-bands of Hurricane Gustav observed at a height of 4 km on September 2, 2008 at 1200 UTC near the mouth of the Mississippi River from the NOAA radar mosaic. The color scale on the far right shows the dBZ values. The broken yellow curve represents the limit of the radar range. ***(center)*** A 100 km wide swath of TerraSAR-X imagery obtained at nearly the same time. The red dashed lines draw attention to comparable features evident in both images.

.

5.2 Precipitation Retrieval over Water

Retrieval of rainfall over sea surfaces is more difficult than that over land because the sea surface is altered by wind roughening and raindrop impact. The wind field that roughens the sea surface around precipitating clouds, and the impinging raindrops that damp surface waves complicate the sea surface structure. Examples of sea surface roughness patterns around precipitation observed by C-band SARs (C-SARs) are shown in Alpers and Melsheimer (2004).

Although the retrieval of marine rainfall from single frequency X-SAR radar cross sections is hobbled by this ambiguity, the problem becomes tractable when C and X-band SARs observe the same scene. The model of Contreras and Plant (2006) was used to compute the relationship between C and X-band values of $\sigma^0(x)$ for wind-roughened, and rain impacted sea surfaces. Those model computations were run for VV and HH polarization, and for incidence angles of 30, 45 and 60 degrees. Various combinations of rainfall rates, 0, 5, 10, and 40 mm/h along with wind speeds values of 3, 4, 5, 10, 15, and 20 m/s at 10m above the sea surface were considered. The viewing directions were up-wind, cross-wind and down-wind. In addition, sea surface cross section measurements for wind-roughened sea surfaces found by Fernandez et al. (2006) were interpolated to yield comparable relationships for 25, 30, 35, 45 m/s with no rain. Those relationships can be fitted by:

$$\sigma^{0X} = f_{X\text{-}C}\ \sigma^{0C} \qquad (3)$$

It is noteworthy that the model data from wind roughened surfaces only, and those from sea surfaces subjected to wind roughening *and* wave damping by rain impact follow common linear trends within ~ 15%. Values for $f_{X\text{-}C}$ for VV polarization at 30°, 45°, and 60° are 1.53, 1.47 and 1.16 respectively, and those for HH polarization are 1.50, 1.88 and 1.42.

Shuttle SAR measurements were made at C and X-band. The C-band NRCS is barely affected by rain so that C-band NRCS measurements can be related to X-band σ^0 values by Eq. (3).

A sample of data presented in Fig. 7 of Melsheimer et al. (1998) was analyzed to demonstrate the use of dual frequency data. The scene in Fig. 4 (upper left) shows a convective cell over water. The NRCS values along the scan A-A' are shown in (upper right) It was noted from various model runs that rainfall had a minor effect on C-band NRCS measurements. (~0.3dB) so that $\sigma_{SAR}{}^{C}(x) \simeq \sigma^{0C}(x)$. The background $\sigma^{0X}(x)$ was thus derived from the application of linear equation (3) to $\sigma^{0C}(x)$ presented in Fig. 7a of Melsheimer et al. (1998). The measured X-band NRCS, and that computed from a model with transformed sea surface NRCS values is shown in Fig. 4 (upper right). The $R(x,z)$ that produces this NRCS scan is shown in Fig. 4 (lower right).

6 THE C- BAND DIFFERENTIAL POLARIZED PHASE SHIFT AS A VALIDATION

Bringi and Chandrasekhar (2001) showed that the Differential Polarized Phase Shift (DPPS) provides a measure of rainfall rate along a propagation path. Although no measurements of the X-band DPPS were available, the C-band DPPS provided some validation of the rainfall rate distribution, $R(x,z)$, derived from the X-band NRCS. The DPPS is determined by the integral of the specific differential phase, K_{dp}, along the two way propagation path, i.e.

$$DPPS(x) = \frac{2}{\sigma_{SAR}\cos\theta}\{ \int_0^{z_0} K_{dp}\left[x(z)\right]\sigma_{srf}\left[x(z)\right]dz + \int_0^{z_0} K_{dp}\left[x'(z')\right]\sigma_{vol}\left[x'(z')\right]dz\} \qquad (4)$$

where z_o is the height of the freezing layer. We used the C-band K_{dp}–R values for raindrops tabulated by Teschl et al. (2006). These were generalized to yield:

$$K_{\mathrm{dp}} = \frac{0.168}{\lambda}\ \sin^2\theta\ \ \mathrm{R}^{1.20} \quad (^{\circ}/\mathrm{km}) \qquad (5)$$

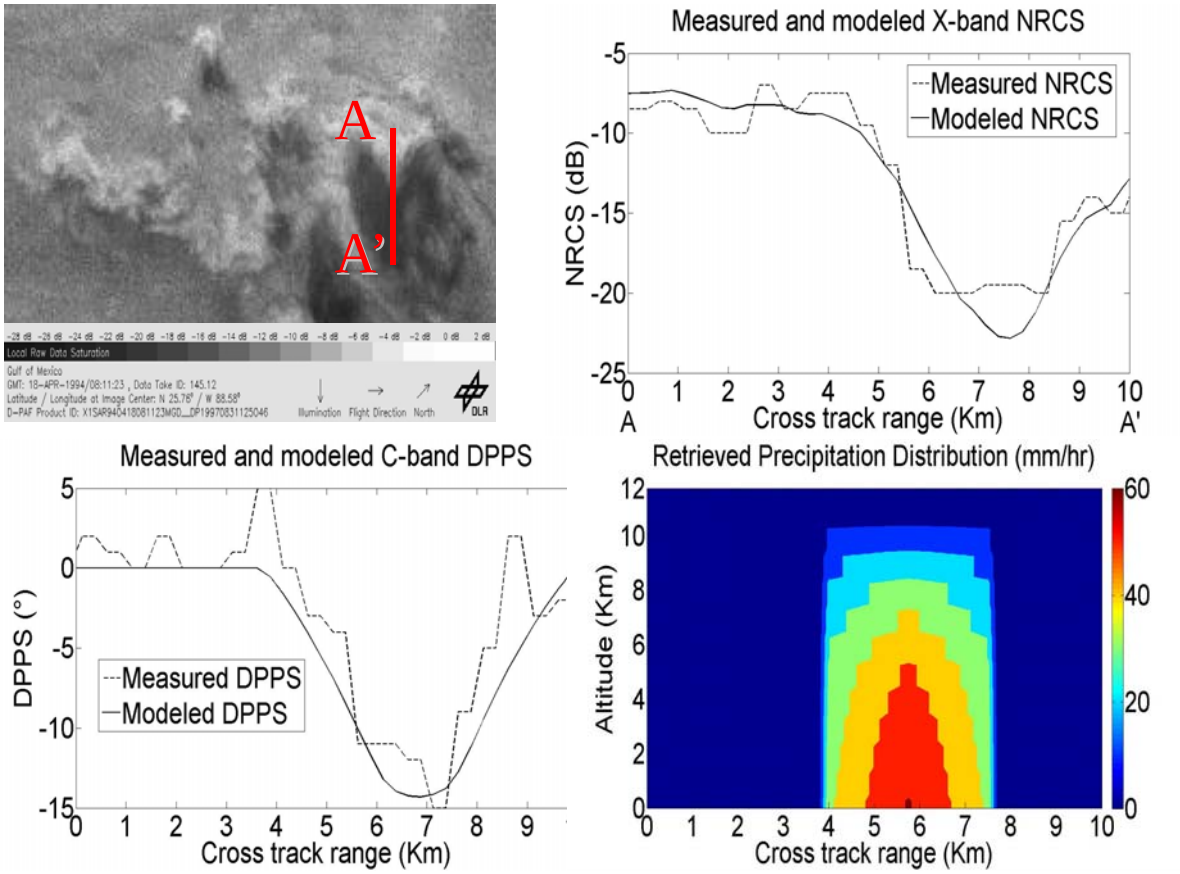

Fig.4 (Upper Left) An X-band image observed over the Gulf of Mexico, 17 April, 1994 at 18:47 UTC during STS-59, first presented in Melsheimer et al. (1998) as part of their Fig. 3. (***Upper Right***) The X-band NRCS scan along the red transect A-A' in Fig. 7a of the Melsheimer et al.(1998) paper (- - - -). The NRCS computed from the model $R(x,z)$ distribution found in our study was (**-------**). The $\sigma^0(x)$ was obtained from the transformed C-band NRCS. ***(Lower Left)*** The model C-band DPPS for the same $R(x,z)$ compared to that presented in Fig. 7d of Melsheimer et al. (1998) (- - - -). The K_{dp}-R relationship was an extrapolation from Teschl et al. (2006) and private communication. ***(Lower Right)*** The $R(x,z)$ distribution used in the model. Note that the width of this cell is ~ 3. km. This cell width is consistent with the along-track dimension shown in the *Upper Left*. This cell would just fill one TRMM PR footprint.

Ryzhkov and Zrnic (1998) found that K_{dp}, for snow was ~0.03 ^{o}/km at S-band. That value was nearly independent of the melted rainfall rate. The K_{dp}, of snow is expected to be about twice that large at C-band. Because of the irregular shape of snow, there was even some uncertainty about the sign of K_{dp},. In view of these considerations, we neglected the effect of snow on the C-band DPPS.

The measured C-band DPPS and that computed from the model are compared in Fig. 4 (lower left) The model computations appear to be consistent with the measurements.

CONCLUSION AND DISCUSSION

Unlike the TRMM PR, which provides highly resolved vertical precipitation profiles, X-SARs mainly measure the slant-path integrated scattering and attenuation produced by precipitation in orthogonal oblique directions. As a consequence, the

algorithms to retrieve rainfall distributions from X-SAR data are more complex than those used for conventional radars. As in all rainfall retrievals from single frequency radar data, numerous simplifying assumptions are needed. Retrieval models over land assumed that the surface below the rain had the same σ^0 as the neighboring surface. (The same assumption used in the TRMM PR surface reference technique). The size distribution of the hydrometeors was assumed to be known. A sharp transition was assumed between rain and snow at the freezing height. No graupel or supercooled water were considered. More realistic assumptions about the precipitation parameters should ultimately be employed. The shadow zone of the NRCS mainly depends on the extinction coefficient of the rain. That quantity is more closely related to the path integrated rainfall rate than the effective radar reflectivity factor, which is widely used for rainfall retrievals from conventional radar studies.

This study employed rainfall retrieval algorithms based on statistical and analytical VIE methods to infer the rainfall distribution over the uniform land surface of the Amazon Basin. Although the techniques are quite distinct, they gave distributions that were in reasonable agreement. However it should be stressed that we had no independent verification of the validity of those retrieved distributions in that case.

The coincident measurements of rain bands in Hurricane Gustav near the Mississippi delta in 2008 by NOAA NEXRAD and TerraSAR-X can provide a validation of the retrieved rainfall distributions. Preliminary analysis suggests that rainfall producing radar reflectivity factors greater than 35 dBZ over land and those more than 20 dBZ over water can be observed by TerraSAR-X.

In spite of the variability of the NRCS of sea surfaces in the proximity of rainfall, we were able to take advantage of the insensitivity of the C-band NRCS to atmospheric rain to infer the C-band NRCS of the sea surface. We found that the C-band NRCS could be transformed to an X-band sea surface NRCS that was used as a boundary condition for the X-band NRCS analysis.

A combined C and X-band retrieval from two satellites in a common polar orbital plane may yield additional information regarding precipitation distributions. One such pair of satellites might be the TerraSAR-X (X-band) and the RadarSAT-2 (C-band). Fig. 5 shows the regions observed by both satellites within ten minutes of each other in the course of a week.

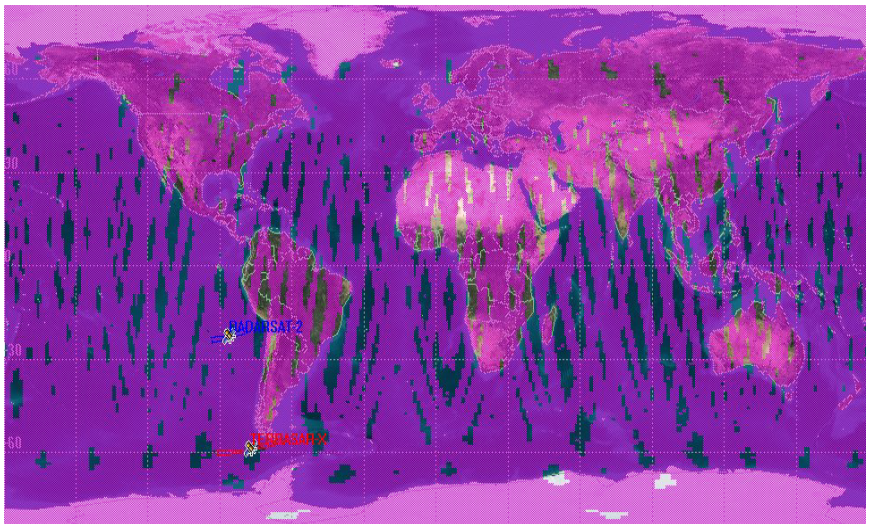

Fig.5 Violet bands show the coverage by both the X and C-band SARs aboard TerraSAR-X and RadarSAT-2 respectively observed within ten minutes of each other. The data are accumulated in the course of a week.

We had measurements of the C-band DPPS. While the measured and modeled DPPS were reasonably consistent, several simplifying assumptions about the K_{dp}, of the various species of hydrometeors were made. More comprehensive polarization measurements would lend more credence to the retrieved results. Once sufficient confidence in the retrievals has been generated, the DPPS and the NRCS could be combined into a future algorithm.

We strongly recommend the establishment of programs to tap into the unique X-SAR data streams as part of the forthcoming Global Precipitation Measurement mission.

Acknowledgments

We thank Messrs. R. Cantelmi and G. Poccia for their computational contributions. We thank Mr. Chito Parong of the AGI Corp. for preparing the illustration of the nearly coincident TerreSAR-X and RadarSAT-2 observation swaths. We also wish to acknowledge graphic support by Ms. Beth Tully. Part of this study was funded by NASA Grant NAG5-9668.

References

Alpers, W. C. Melsheimer, 2004: Rainfall, *Synthetic Aperture Radar Marine Users Manual,* U.S. Dept. of Commerce, NOAA, pp 353-372.

Atlas, D., R.K. Moore, 1987: The measurement of precipitation with synthetic aperture radar. *J. Atmos. and Ocean Tech*., **4**, 368-376.

Bennartz, R., G.W. Petty, 2001: The sensitivity of microwave remote sensing observations of precipitation to ice particle size distributions. *J. of Appl. Met*., **4,** 345-364.

Bringi, V.N., V. Chandrsekar, 2001: *Polarimetric Doppler Weather Radar*, Cambridge University Press, pp 636.

Buckreuss, S., W. Balzer; P. Muhlbauer, R. Werninghaus, W. Pitz, 2003: The TerraSAR-X satellite project. *Proc. of the Intern. Geosci. and Remote Sensing Symp.*, (IGARSS03), 3096 – 3098.

Caltagirone, F., G. Angino, F. Impagnatiello, A. Capuzi, S. Fagioli, R. Leonardi, 2007: COSMO-SkyMed: An advanced dual system for Earth observation, *Proc. of the Intern. Geoscience and Remote Sensing Symp.* (IGARSS07), Barcelona (E), 23-27 July.

Contreras, R.F., W.J. Plant, 2006: Surface effect of rain on microwave backscatter from the ocean: Measurement and modeling, *J. Geophys. Res.*, **111**, C08019

Durden, S.L., Z.S. Haddad, A. Kitiyakara, F.K. Li, 1998: Effects of non-uniform beam filling on rainfall retrieval for the TRMM Precipitation Radar. *J. Ocean and Atmos. Tech*., **15**, 635-646.

Fernandez, D.E., J.R. Carswell, S. Frasier, P.S. Chang, P.G. Clark, F.D. Marks, 2006: Dual-polarized C- and Ku-band ocean backscatter response to hurricane-force winds, *J. Geophys. Res.*, **111**, C08013.

Jameson, A.R., F.Li, S.L. Durden, Z.S. Haddad, B. Holt, T. Fogary, E. Im, R.K. Moore 1997: SIR-C/X-SAR Observations of rainstorms. *Remote Sens. Environ*, **59**, 267-279.

Jordan, R.L., B.L. Huneycutt, M. Werner, 1995: The SIR-C/X SAR synthetic aperture radar system. *IEEE Trans. Geosci. and Remote Sensing*, **33**, 829-839.

Kummerow, C., et al. 2000: The status of the Tropical Rainfall Measuring Mission (TRMM) after two years in orbit. *J. Appl. Meteor.*, **39**, 1965-1982.

Marzano, F.S. , J. A. Weinman, A. Mugnai, N. Pierdicca 2006: Rain retrieval over land from X-band space-borne synthetic aperture radar: a model study. Presentation at the *Fourth European Conference on Radar Meteorology and Hydrology, ERAD06*, Barcelona Sept. 18-21.

Marzano, F.S., J.A. Weinman 2008: Inversion of space-borne X-Band Synthetic Aperture Radar measurements for precipitation remote sensing over land. *Trans. on GeoSci. and Rem. Sensing* **46,** 3472-3487

Melsheimer, C., M. Gade, and W. Alpers, 1998: Investigation of multifrequency/ multi-polarization radar signatures of rain cells derived from SIR-C/X-SAR data. *J. Geophys. Res.,* **103**, 18,867-18,884.

Moore, R. K., A. Mogili, Y. Fang, B. Beh, A. Ahamad, 1997: Rain measurement with SIR-C/X-SAR data. *Remote Sensing of Environment*, **59**, 280-293.

Pichugin, A.P., Yu. G. Spiridonov 1991: Spatial distributions of rainfall intensity recovery from space radar images. *Sov. J. Remote Sensing*, **8**, 917-932.

Ryzhkov, A.V., D.S. Zrnic, 1998: Discrimination between rain and snow with a polarization radar*, J. Appl. Met*., **37**, 1228-1240

Sharay, Y., U. Naftaly, 2006: "TecSAR: design considerations and programme status," *IEE Proceedings- Radar, Sonar and Navigation,* , *ISSN: 1350-2395*, **153**, Issue 2, 117-121

Teschl, F.; Randeu, W. L.; Schönhuber, M.; Teschl, R. 2006: Simulation of the specific differential phase (KDP) from 2D- Video-Distrometer measurements at S- and C-band wavelengths Paper 61P1.16, *ERAD2006 Conference*, Barcelona, Spain 9/ 18-22 .

Weinman, J.A., F.S. Marzano, 2008: An exploratory study to derive precipitation over land from X-band synthetic aperture radar measurements. *J. Appl. Met.,* **47**, 562-575.

Yuter, S.E., R. A. Houze, 1995: Three-dimensional kinematic and microphysical evolution of Florida cumulonimbus. Part II: Frequency distributions of vertical velocity, reflectivity, and differential reflectivity. *Mon. Wea. Rev*., **123**, 1941-1963.